Available online at www.sciencedirect.com
ScienceDirect
Trans. Nonferrous Met. Soc. China 31(2021) 2522−2531
Transactions of Nonferrous Metals Society of China
www.tnmsc.cn

Physicochemical properties of DMI−$LiNO_3$ solvated ionic liquid and its application in electrodeposition of neodymium at room temperature

Ai-min LIU[1], Yu YAO[1], Meng-xia GUO[1], Yu-bao LIU[2], Zhong-ning SHI[3], Feng-guo LIU[1], Xian-wei HU[1], Wen-cai HE[1], Zhao-wen WANG[1]

1. Key Laboratory for Ecological Metallurgy of Multimetallic Mineral (Ministry of Education), Northeastern University, Shenyang 110819, China;
2. State Key Laboratory of Baiyunobo Rare Earth Resource Researches and Comprehensive Utilization, Baotou Research Institute of Rare Earths, Baotou 014030, China;
3. State Key Laboratory of Rolling and Automation, Northeastern University, Shenyang 110819, China

Received 24 July 2020; accepted 14 January 2021

Abstract: The density, conductivity, and viscosity of the 1,3-dimethyl-2-imidazolinone and lithium nitrate (DMI−$LiNO_3$) solvated ionic liquid were measured as a function of temperature. Additionally, the electrochemical mechanism and electrodeposition of neodymium from the DMI−$LiNO_3$ solvated ionic liquid were investigated. Cyclic voltammetry results indicate that the electrochemical reduction of Nd(III) is irreversible and proceeds via one-step with three-electron transfer, which is controlled by diffusion with a diffusion coefficient of 5.08×10^{-8} cm^2/s. Energy-dispersive X-ray spectrometry and X-ray photoelectron spectroscopy data confirm that the electrodeposit obtained after electrodeposition at −4 V (vs Ag) using the DMI−$LiNO_3$−$Nd(CF_3SO_3)_3$ solvated ionic liquid contains metallic neodymium.

Key words: electrodeposition; neodymium; ionic liquid; physicochemical properties; cyclic voltammetry

1 Introduction

Rare earth (RE) elements are known as industrial vitamins and “mother of new materials” because of their outstanding optical and electro-magnetic properties [1−3]. As the additive, RE elements can significantly improve the qualities and performances of materials with a wide range of properties [4]. Therefore, RE metals have been widely used in fields such as metallurgy, machinery, petrochemical industry, and aerospace. Currently, molten salt electrolysis in LiF−REF_3−RE_2O_3 electrolytes at 1273−1373 K has been applied for RE metal production in the industry, but it is limited by the high electrolysis temperature and low energy efficiency [5,6]. Therefore, identifying a suitable electrolyte from which RE metals can be produced at low temperatures or room temperature is desirable.

Ionic liquids have the advantages such as low melting points, wide electrochemical window, good thermal stabilities, and high electrical conductivities. Thus, the application of ionic liquids for the electrodeposition of RE metals (particularly La and Nd) has been extensively studied. For example, TSUDA et al [7] found that the solubility of $LaCl_3$ increased with an increase in the acidity of aluminum chloride−1-ethyl-3-methylimidazolium chloride ($AlCl_3$−EMICl) ionic liquid, and metallic La was electrodeposited at −1.95 V (vs Al) with LiCl and $SOCl_2$ as additives. LEGEAI et al [8]

Corresponding author: Zhong-ning SHI, Tel: +86-24-83686381, E-mail: znshi@mail.neu.edu.cn
DOI: 10.1016/S1003-6326(21)65672-8

reported that the electrochemical window of the 1-octyl-1-methyl-pyrrolidinium bis(trifluoro methyl-sulfonyl)imide (OMPTf_2N) ionic liquid was 4.8 V (vs Ag/AgCl), and a La film with 350 nm-thickness was formed by electrodeposition method at −1.5 V (vs Ag/AgCl) for 2 h. KIM et al [9] investigated the electrochemical behavior of La(III) in 1-ethyl-3-methyl-imidazolium tetrafluoroborate ([EMIM]-[BF_4]) ionic liquid with 0.1 mol/L LiCl as an additive, and the results suggested that the reduction of La(III) was an irreversible one-step process controlled by the diffusion with a diffusion coefficient of $(1.07−1.19)\times10^{-6}$ cm^2/s.

KONDO et al [10] studied the electrochemical behavior of Nd(III) in triethyl-pentyl-phosphonium bis(trifluoromethyl-sulfonyl)amide ([P_{2225}][TFSA]) ionic liquid, and the diffusion coefficient of Nd(III) at 373 K was of the order of 10^{-7} cm^2/s. Fine and uniform Nd particles were electrodeposited on a copper substrate at −1.95 V (vs Pt) and identified by X-ray photoelectron spectroscopy (XPS). OTA et al [11] investigated the electrochemical behavior of Nd(III) in [P_{2225}][TFSA] using cyclic voltammetry and electrochemical quartz crystal microbalance (EQCM). A clear cathode peak was observed at −2.79 V (vs Pt) with a mass change of 140.4 g/mol, which was close to the theoretical value (144.2 g/mol) for the electrochemical reaction $[Nd(TFSA)_5]^{2-}+3e\rightarrow Nd+5[TFSA]^-$. In addition, metallic Nd could be electrochemically recovered from the waste of Nd−Fe−B magnets using [P_{2225}][TFSA] ionic liquid as the electrolyte [12]. MATSUMIYA et al [13] studied the electrochemical mechanism of Nd(III) in N,N-diethyl-N-methyl-N-(2-methoxyethyl) ammonium bis(trifluoromethyl-sulfonyl) amide ([DEME] [TFSA]) ionic liquid, and the reduction of Nd(III) was an irreversible one-step process controlled by the diffusion with a diffusion coefficient of 1.35×10^{-9} cm^2/s at 353 K. The electrodeposits obtained at −3.40 and −3.60 V (vs Ag) on a copper substrate were mixtures of neodymium and its oxide.

Considering the electrodeposition of RE alloys, numerous studies have been carried out in eutectic solvents by induced co-deposition. For instance, GUO et al [14,15] and LIU et al [16] prepared a series of RE−transition metal alloys including La−Co, La−Ni, and Nd−Fe alloys via induced co-deposition in the acetamide−urea−NaBr melts. The maximum mass fractions of RE metals in the deposited La−Co, La−Ni, and Nd−Fe alloys were 66.32%, 78.81%, and 60.4%, respectively. YANG et al [17] studied the electrochemical behavior and nucleation mechanism of Ni(II) and La(III) in 1-ethyl-3-methylimidazolium chloride−ethylene glycol (EMIC−EG) eutectic ionic liquid, while inductively coupled plasma-atomic emission spectrometry (ICP-AES) and X-ray diffraction (XRD) analyses showed that Ni−La alloys containing 0.2−9.48 wt.% La were deposited at current densities of 3−7 mA/cm^2.

In summary, RE metals can be electrodeposited in ionic liquids such as $AlCl_3$−EMICl, OMPTf_2N, [EMIM][BF_4]−LiCl, [P_{2225}][TFSA], and [DEME][TFSA]. However, $AlCl_3$-based ionic liquids show disadvantage of high hygroscopicity, while other conventional ionic liquids have drawbacks such as high cost and synthetic complexity [18]. Eutectic solvents are inexpensive and suitable for the preparation of RE alloys, but it is difficult to produce pure RE metals because their electrochemical windows are narrow. Recently, ZHANG et al [19] have developed a novel 1,3-dimethyl-2-imidazolidinone−lithium nitrate (DMI−$LiNO_3$) solvated ionic liquid, which was air stable and readily available with a wide electrochemical window. Furthermore, XRD and XPS characterization confirmed that metallic La could be electrochemically deposited on a highly pure Al substrate at –2.3 V (vs Ag) from the DMI−$LiNO_3$ solvated ionic liquid containing $LaCl_3$. In this study, the physical properties including density, conductivity, and viscosity of the DMI−$LiNO_3$ solvated ionic liquid were measured at different temperatures. In addition, the electrochemical mechanism of Nd(III) reduction was investigated by cyclic voltammetry, and the coatings obtained by potentiostatic electrodeposition were analyzed.

2 Experimental

DMI (99%) and $LiNO_3$ (99.9%) were purchased from Shanghai Aladdin Bio-Chem Technology Co., Ltd., while neodymium trifluoromethanesulfonate ($Nd(CF_3SO_3)_3$, 98%) was purchased from Alfa Aesar Chemical Co., Ltd., China. Owing to the high hygroscopicity of $LiNO_3$, the DMI−$LiNO_3$ solvated ionic liquid was prepared in a glove box. The contents of water and oxygen in

the glove box were kept below 0.0001%. Firstly, the DMI solvent was added to a beaker and heated on a magnetic heating plate. Then, $LiNO_3$ was slowly added to DMI, and the mixture was heated with magnetic stirring until a homogeneous clear liquid containing 0.5 mol/L $LiNO_3$ was formed. Finally, 0.05 mol/L $Nd(CF_3SO_3)_3$ was dissolved in the DMI−$LiNO_3$ solvate ionic liquid for Nd electrodeposition.

The physicochemical properties of the DMI−$LiNO_3$ solvated ionic liquid were measured in a glove box. The densities of the ionic liquid at room temperature (298 K) to 358 K were measured using the Archimedes method, where the calibration was performed using deionized water. The electrical conductivities were measured using the fixed conductivity cell method by employing an LCR meter (Agilent 4263B; Agilent Technologies, Palo Alto, USA), which was calibrated using a standard potassium chloride solution (1 mol/L KCl). The viscosities were measured using a Ubbelohde viscometer (HAD−1834; Heng Odd Instrument, Beijing, China).

Cyclic voltammetry experiments were performed using an electrochemical workstation (CHI600E; CH Instruments, Shanghai, China). A tungsten wire (99.95%) with an immersion area of 0.8 cm^2 was selected as the working electrode, while platinum (99.99%) and silver (99.99%) wires with a diameter of 0.5 mm were used as the counter and reference electrodes, respectively. The electrochemical workstation was also used to perform electrodeposition experiments using a three-electrode system. The working electrode comprised an aluminum sheet (99.99%), while the counter electrode and reference electrode constituted a tungsten sheet (99.99%) and a silver wire (99.99%), respectively. The electrodes used before each experiment were polished using sandpaper and cleaned with deionized water. The phase compositions of the products were analyzed by XRD (D8 Advance; Bruker, Karlsruhe, Germany), and the morphologies and elemental compositions of the products were determined by scanning electron microscopy (SEM, Ultra Plus; Zeiss, Oberkochen, Germany) coupled with an energy-dispersive X-ray spectroscopy (EDS) system. In addition, the electrodeposits were characterized using XPS (Axis Ultra DLD, Kratos, Japan).

3 Results and discussion

3.1 Physical properties of ionic liquid

The densities of the DMI solvent and DMI−$LiNO_3$ solvated ionic liquid (containing 0.5 mol/L $LiNO_3$) were measured using the Archimedes method at 298−358 K. As shown in Fig. 1, the density of DMI decreases from 1.064 to 1.021 g/cm^3 with an increase in temperature from 298 to 358 K, while the density of the DMI−$LiNO_3$ solvated ionic liquid decreases from 1.133 to 1.087 g/cm^3. The addition of $LiNO_3$ to the DMI solvent results in an increase in its density. The decrease in density with increasing temperature is mainly due to an increase in the thermal motion of the particles as the number of particles per unit volume decreases with increasing temperature [20,21]. Moreover, the density of the DMI−$LiNO_3$ solvated ionic liquid (ρ, g/cm^3) is linearly correlated to temperature (T, K), as described by Eq. (1).

$$\rho=-7.64\times10^{-4}T+1.36 \quad (1)$$

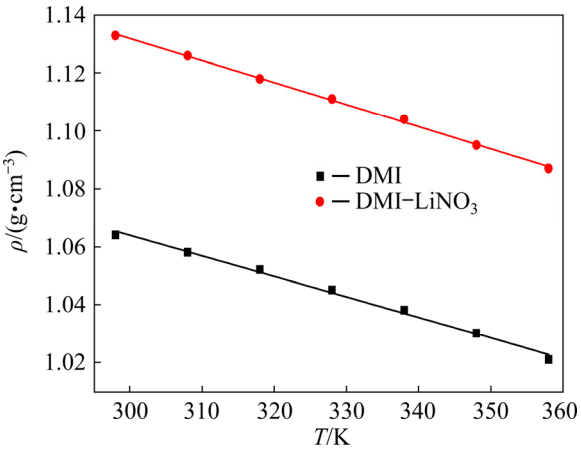

Fig. 1 Densities of DMI solvent and DMI−$LiNO_3$ solvated ionic liquid at different temperatures

The conductivities of the DMI solvent and DMI−$LiNO_3$ solvated ionic liquid (containing 0.5 mol/L $LiNO_3$) at 301−350 K are shown in Fig. 2(a). With an increase in temperature from 301 to 350 K, the conductivity of DMI increases from 0.04 to 0.11 mS/cm, while the conductivity of the DMI−$LiNO_3$ solvated ionic liquid increases from 1.02 to 6.14 mS/cm. The addition of $LiNO_3$ to DMI results in an obvious increase in conductivity. The conductivity increases with an increase in temperature because of a decrease in the viscosity

and increase in the diffusion or migration rate of ions at high temperature. Moreover, the conductivity of the DMI−$LiNO_3$ solvated ionic liquid at 318 K is 1.78 mS/cm, which is of the same order of magnitude for the values of conventional ionic liquids such as urea−acetamide−$AlCl_3$ (1.5 mS/cm at 323 K), N-propyl-N-methyl pyrrolidinium bis(trifluoro methanesulfonyl)imide (2.3 mS/cm at 298 K), and [BMIM][BF_4] (3.5 mS/cm at 298 K) [22−24].

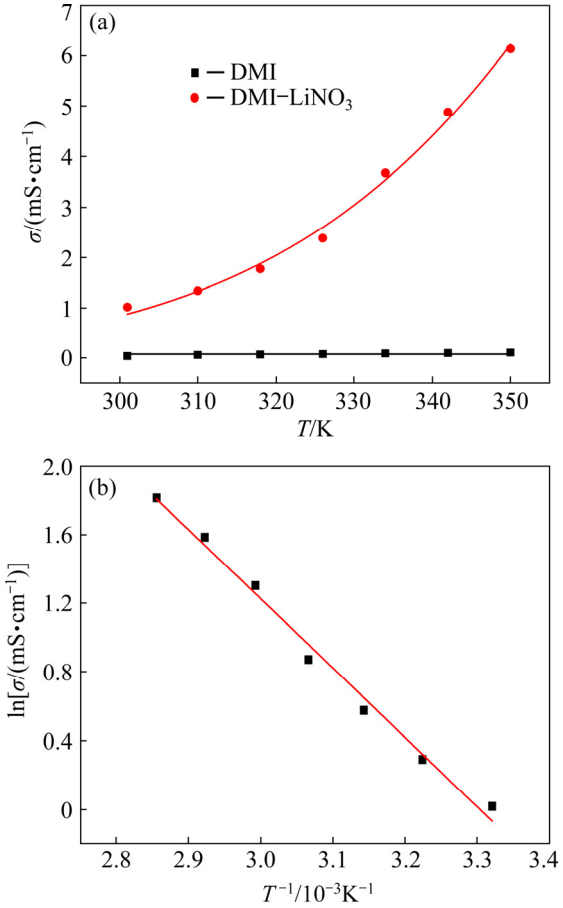

Fig. 2 Conductivities (σ) of DMI solvent and DMI−$LiNO_3$ solvated ionic liquid at different temperatures (a) and relationship between ln σ and T^{-1} for DMI−$LiNO_3$ solvated ionic liquid (b)

Arrhenius equation is generally applied to determining the transport properties in non-aqueous solutions including the molten salts and ionic liquids, and the relationship between conductivity and temperature can be described by Eq. (2) [25]:

$$\ln \sigma = \ln \sigma_0 - E_a/(RT) \quad (2)$$

where σ is the conductivity (mS/cm); σ_0 is the pre-exponential factor (mS/cm); E_a is the diffusion activation energy (J/mol); R is the mole gas constant (8.314 J/(mol·K)); T is the experimental temperature (K). As shown in Fig. 2(b), the logarithmic conductivity of the DMI−$LiNO_3$ solvated ionic liquid (ln σ) is linearly related to the reciprocal of temperature (T^{-1}). Based on Eq. (2) and the slope of the plot in Fig. 2(b), the diffusion activation energy for the DMI−$LiNO_3$ solvated ionic liquid is 33.53 kJ/mol. Therefore, conductivity as a function of temperature can be expressed by Eq. (3):

$$\sigma = 611530.43\exp(-4032.58/T) \quad (3)$$

The viscosities of DMI solvent and DMI−$LiNO_3$ solvated ionic liquid (containing 0.5 mol/L $LiNO_3$) at 298−348 K were measured using a viscometer. As shown in Fig. 3(a), viscosity of DMI is significantly lower than that of the DMI−$LiNO_3$ solvated ionic liquid. The viscosity of DMI at 298 K is 1.93 mPa·s, which is consistent with the viscosities of general organic solvents. After the addition of 0.5 mol/L $LiNO_3$ to DMI, the viscosity

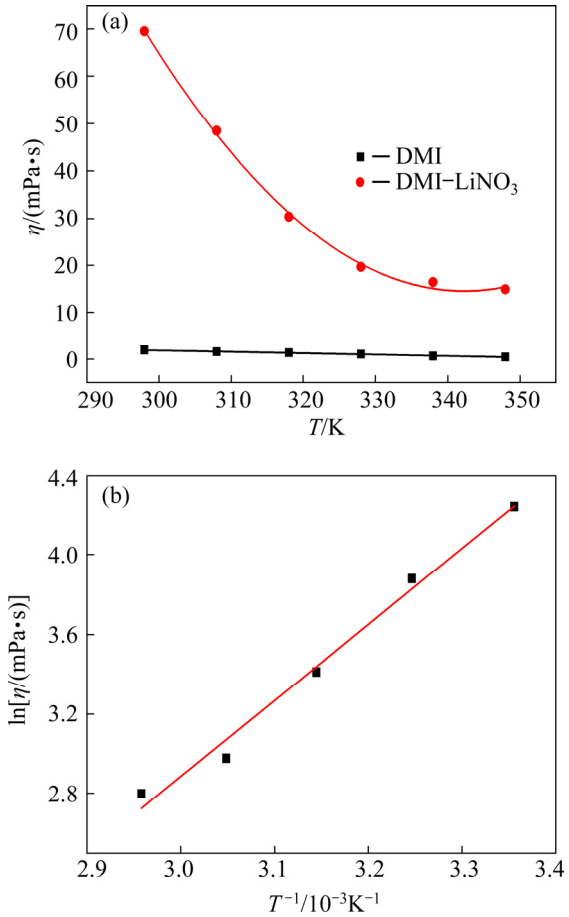

Fig. 3 Viscosities (η) of DMI solvent and DMI−$LiNO_3$ solvated ionic liquid at different temperatures (a) and relationship between ln η and T^{-1} for DMI−$LiNO_3$ solvated ionic liquid (b)

at 298 K significantly increases to 69.59 mPa·s, indicating that the structure of the electrolyte changes from the initial molecular solvent to that of an ionic liquid. The viscosity of the DMI−$LiNO_3$ solvated ionic liquid increases upon the addition of $LiNO_3$ because of an increase in ionic association and decrease in the mobility of the $[Li(DMI)_n]^+$ solvated species [19,26]. BARGHAMADI et al [27] investigated the effect of $LiNO_3$ additive on the viscosity of several ionic liquids, and the viscosity of 1,2-dioxolane and 1,2-dimethoxyethane solvent with 1 mol/kg lithium bis(trifluoromethanesulfonyl)imide increased from 2.9 to 3.6 mPa·s after the addition of 0.1 mol/kg $LiNO_3$ at 296 K. In addition, the viscosity of the DMI−$LiNO_3$ solvated ionic liquid is lower than those of some conventional ionic liquids and deep eutectic solvents because the latter have lower conductivities compared to electrolytes containing organic solvents [27]. For example, the viscosities of 1-butyl-1-methyl pyrrolidinium bis(trifluoromethylsulfonyl) imide([BMPyrr][NTf_2]) ionic liquid, [BMIM][BF_4] ionic liquid, and choline chloride−urea deep eutectic solvent at 298 K are 72.57, 100.66, and 748.09 mPa·s, respectively [28−30].

Furthermore, the viscosity of the DMI−$LiNO_3$ solvated ionic liquid decreases from 69.59 to 14.89 mPa·s upon an increase in temperature from 298 to 348 K owing to the effect of temperature on hydrogen bonds and van der Waals forces. As described in Eq. (4), the viscosities at various temperatures can be fitted to the Arrhenius equation [21,31].

$$\ln \eta = \ln \eta_\infty - E_\eta/(RT) \quad (4)$$

where η_∞ is the viscosity at infinite temperature (mPa·s), and E_η is the apparent activation energy (J/mol). As shown in Fig. 3(b), the logarithmic viscosity ($\ln \eta$) is linearly related to the reciprocal of temperature (T^{-1}). The fitting parameters η_∞ and E_η are determined to be 1.86×10^{-4} mPa·s and 31.81 kJ/mol, respectively. Therefore, the viscosity can be described by $\ln \eta = -8.59 + 3825.7/T$

3.2 Cyclic voltammetry

The cyclic voltammetry curves of the DMI−$LiNO_3$ solvated ionic liquid in the absence and presence of $Nd(CF_3SO_3)_3$ were obtained using a tungsten electrode (Fig. 4). The scan rate was 80 mV/s, and the experimental temperature was 303 K. As shown in Fig. 4(a), during the sweep from 0 to −5 V (vs Ag), the cyclic voltammetry curve of DMI is very stable, indicating its high stability. After the addition of 0.5 mol/L $LiNO_3$ to DMI, a pair of reduction and oxidation signals are observed, as shown in Fig. 4(b). Based on the results of our previous study, the current waves *P*–*P′* are due to the reduction and oxidation of Li, and the appearance of the cathodic current loop indicates the nucleation of Li on the tungsten working electrode [19]. The shoulders in the cathodic scan at approximately −2.6 V (vs Ag) and anodic scan at −1.1 V (vs Ag) are observed, which may be related to the underpotential deposition of Li and its oxidation on the working electrode [32]. In addition, no noticeable impurity peak is observed in the cyclic voltammetry curve of the DMI−$LiNO_3$ solvated ionic liquid from 0 to −2.8 V (vs Ag), indicating that the ionic liquid is stable within this potential range.

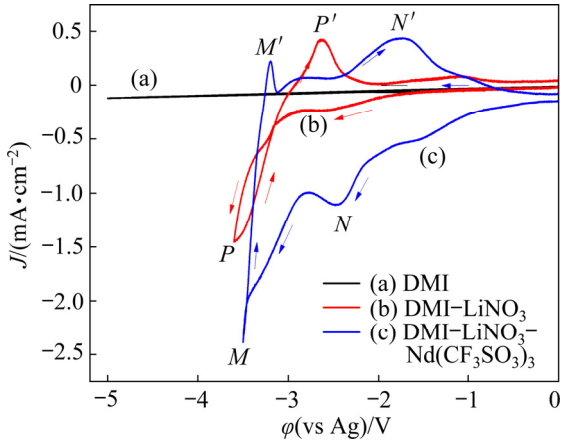

Fig. 4 Cyclic voltammetry curves of DMI (a), DMI−$LiNO_3$ (b), and DMI−$LiNO_3$−$Nd(CF_3SO_3)_3$ (c) solvated ionic liquid at 303 K and scan rate of 80 mV/s

Figure 4(c) shows the cyclic voltammetry curve of the DMI−$LiNO_3$ solvated ionic liquid containing 0.05 mol/L $Nd(CF_3SO_3)_3$. Two pairs of reduction and oxidation peaks (*M*–*M′* and *N*–*N′*) are observed. Considering the cyclic voltammetry curve in the absence of $Nd(CF_3SO_3)_3$, the current density increase at approximately −1.0 V (vs Ag) and the subsequent reduction peak at −2.5 V (Point *N*) are attributed to the electrodeposition of Nd. The second reduction peak *M* (−3.5 V) is due to the reduction of Li^+ ions to metallic Li. During the reverse potential sweep, the oxidation peaks *M′* (−3.2 V) and *N′* (−1.7 V) are related to the anodic

stripping of Li and Nd from the surface of the working electrode, respectively.

To investigate the kinetics of Nd electrodeposition, cyclic voltammetry tests were performed at different scan rates (20, 40, 60, 80, and 120 mV/s). As shown in Fig. 5, the potentials of the reduction peaks gradually shift toward more negative values with increasing the scan rate. For the reversible electrode reaction, the peak potential (φ_p) is independent of the scan rate (v). Therefore, the electrochemical reduction of Nd(III) on tungsten electrode in DMI−$LiNO_3$−$Nd(CF_3SO_3)_3$ solvated ionic liquid can be considered an irreversible process.

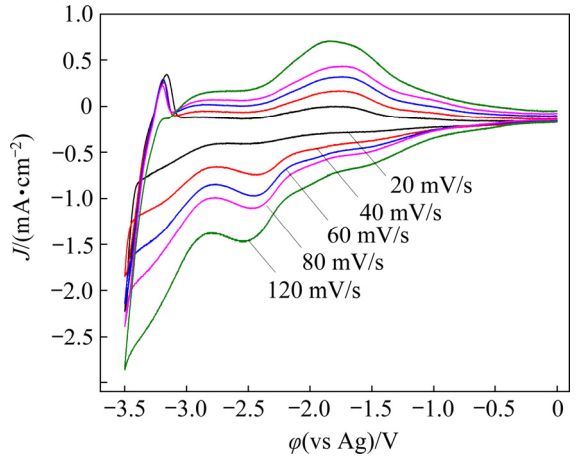

Fig. 5 Cyclic voltammetry curves of DMI−$LiNO_3$−$Nd(CF_3SO_3)_3$ solvated ionic liquid at 303 K and scan rates of 20, 40, 60, 80, and 120 mV/s

For an irreversible electrochemical reaction, the number of electrons transferred can be calculated using the following equation [33]:

$$\varphi=B-[RT/(nF)]\ln[I/(I_p-I)] \quad (5)$$

where φ is the potential (V), B is the half-wave potential (V), n is the number of transferred electrons, F is the Faraday constant (96485 C/mol), I is the current (A), and I_p is the current of the reduction peak (A). The relationship between potential (φ) and $\ln[I/(I_p-I)]$ at 303 K is plotted based on the data derived from Fig. 5. As shown in Fig. 6(a), there is a linear relationship between φ and $\ln[I/(I_p-I)]$. Combining the slopes of the plot in Fig. 6(a) and Eq. (5), the number of transferred electrons is 3.2, which is close to the theoretical number of transferred electrons in the reduction of Nd(III) to metallic Nd. Therefore, the reduction of Nd(III) in the DMI−$LiNO_3$−$Nd(CF_3SO_3)_3$ solvated ionic liquid proceeds via one-step three-electron transfer, and the electrochemical reaction can be described by Eq. (6):

$$Nd(III)+3e=Nd \quad (6)$$

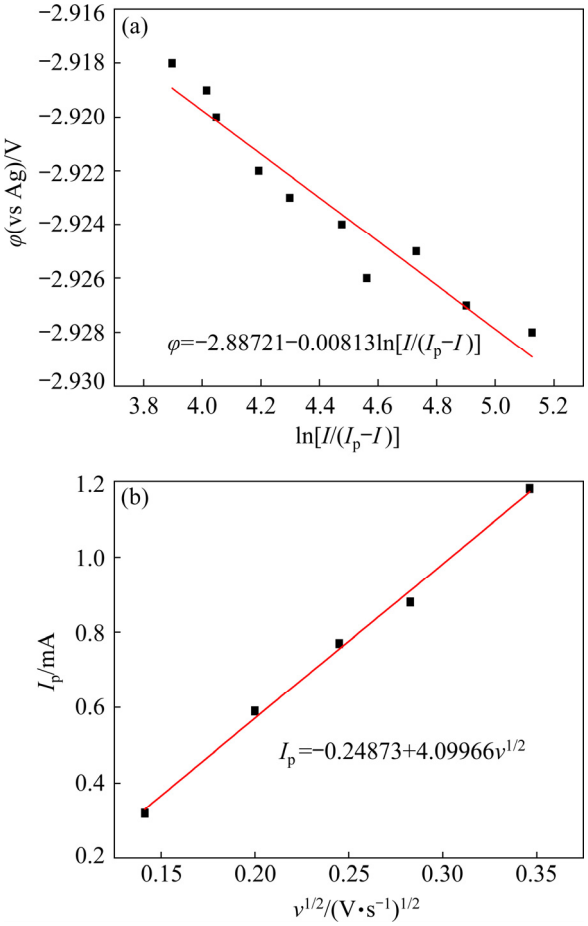

Fig. 6 Relationships between φ and $\ln[I/(I_p-I)]$ (a), and I_p and $v^{1/2}$ (b)

For an irreversible electrode process, there is a linear relationship between $|\varphi_p-\varphi_{p/2}|$ and the charge transfer coefficient (α) [33]. Based on the data derived from Fig. 5 and Eq. (7), the charge transfer coefficient α at different scan rates can be calculated, and the average value of α for Nd(III) reduction in DMI−$LiNO_3$−$Nd(CF_3SO_3)_3$ solvated ionic liquid is 0.087.

$$|\varphi_p-\varphi_{p/2}|=1.857RT/(\alpha nF) \quad (7)$$

where φ_p is the peak potential of Nd(III) reduction (V), and $\varphi_{p/2}$ is the half-peak potential of Nd(III) reduction (V).

Furthermore, the peak current density of Nd(III) reduction in Fig. 5 gradually changes from −0.40 to −1.48 mA/cm^2 with an increase in the scan rate from 20 to 120 mV/s. As shown in Fig. 6(b), a

linear relationship is observed between the peak current (I_p) and square root of the scan rate ($v^{1/2}$), indicating that Nd electrodeposition is controlled by diffusion [17]. According to the Randles−Sevcik equation (Eq. (8)) and the slope of the plot in Fig. 6(b), the diffusion coefficient for Nd(III) reduction on tungsten electrode in the DMI−$LiNO_3$−$Nd(CF_3SO_3)_3$ solvated ionic liquid is calculated to be 5.08×10^{-8} cm^2/s [33].

$$I_p=0.4958nFAc_0D^{1/2}v^{1/2}[\alpha nF/(RT)]^{1/2} \quad (8)$$

where A is the immersion area of the working electrode (0.8 cm^2), c_0 is the bulk concentration of Nd(III) ions (5×10^{-5} mol/L), and D is the diffusion coefficient (cm^2/s).

3.3 Characterization of electrodeposits

Owing to the pre-deposition of metals on the reactive Al substrate, Al−Nd intermetallic compounds can be easily formed by electrodeposition on Al electrode [18,19]. Therefore, electrodeposition experiments in the DMI−$LiNO_3$−$Nd(CF_3SO_3)_3$ solvated ionic liquid were carried out on an Al substrate to ensure the electrochemical extraction of metallic Nd. The applied potential was −4 V (vs Ag), and the deposition time was 2 h.

The phase composition of the electrodeposit was determined by XRD. As shown in Fig. 7(c), the XRD pattern indicates that the cathode product is composed of Al, Li, and LiAl phases. Among these, the Al phase is attributed to the cathode, while the Li and LiAl phases are formed because the applied potential is sufficiently negative for the electrochemical reduction of Li^+ ions. The SEM image and EDS spectrum of the coating are shown in Figs. 7(a) and (b), respectively. The Li particles are distributed on the coating surface. The EDS data show that the electrodeposit mainly contains Al and O, and Li is not detected within the resolution of the EDS detector because the atomic number and energy of Li are small. In addition, the electrodeposit was analyzed by XPS, and the results are shown in Fig. 7(d). According to the fine scan of the Li peak, zero-valent Li with a mass fraction of 24.77% was detected [34], indicating that metallic Li is obtained by electrodeposition at −4 V (vs Ag) in the DMI−$LiNO_3$ solvated ionic liquid.

Furthermore, the electrodeposition experiment was performed in the DMI−$LiNO_3$ solvated ionic liquid containing 0.05 mol/L $Nd(CF_3SO_3)_3$ on an Al substrate with an applied potential of −4 V (vs Ag). The SEM image and EDS spectrum of the electrodeposit are shown in Fig. 8. The EDS spectra show that the particles with agglomerated structures

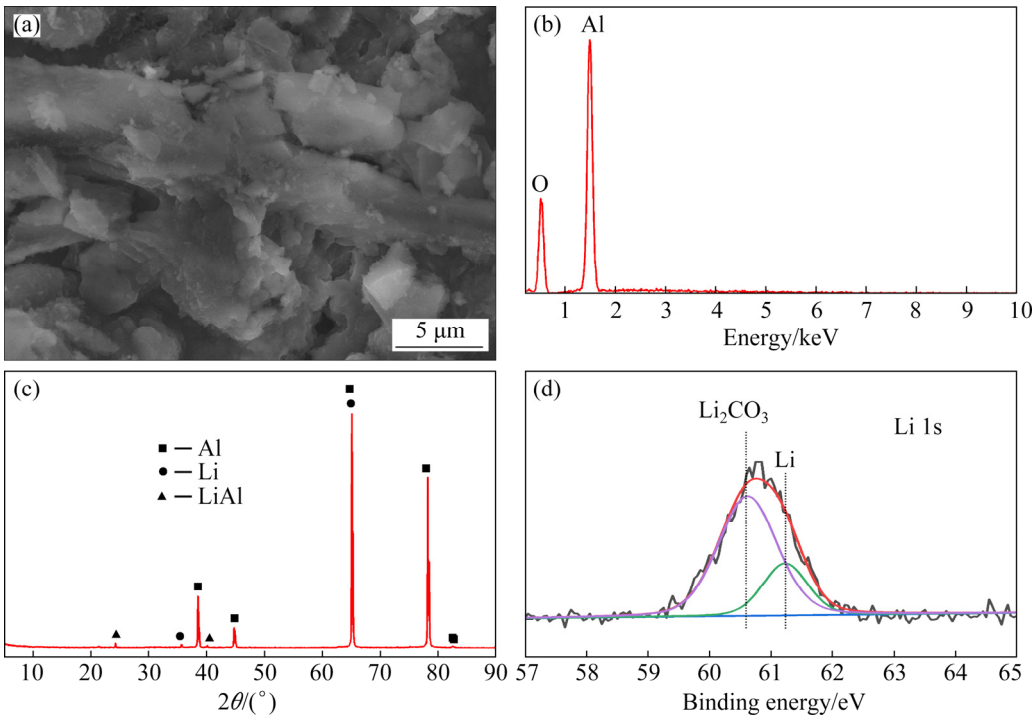

Fig. 7 SEM image (a), EDS spectrum (b), XRD pattern (c) and XPS data (d) of electrodeposits obtained from DMI−$LiNO_3$ solvated ionic liquid on Al substrate after electrodeposition at −4 V (vs Ag) for 2 h

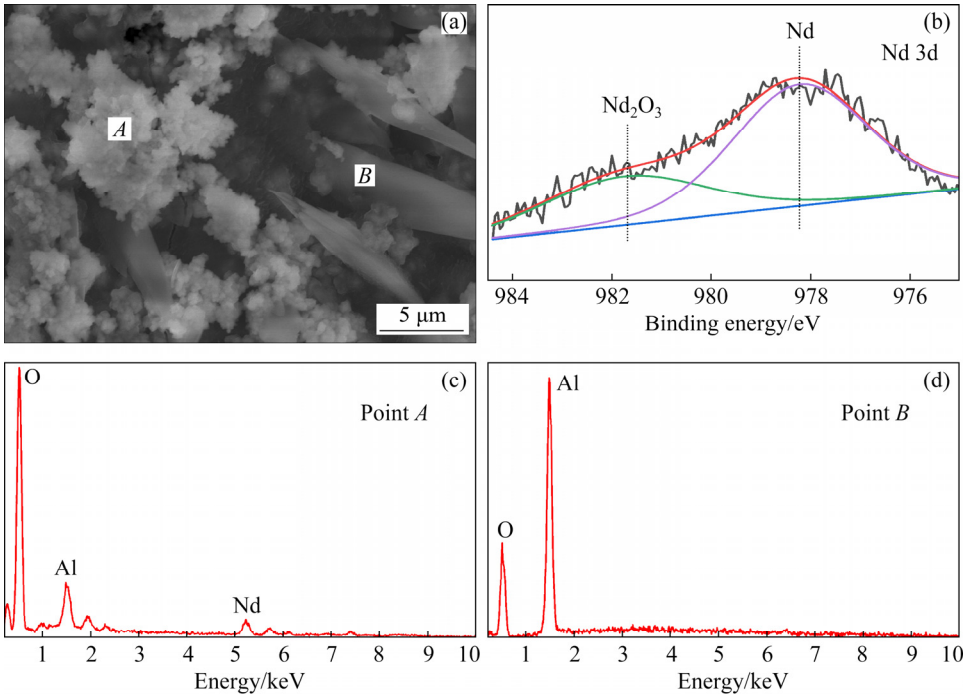

Fig. 8 SEM image (a), XPS spectrum (b), and EDS data (c, d) of electrodeposit obtained from DMI−$LiNO_3$−$Nd(CF_3SO_3)_3$ solvate ionic liquid after electrodeposition at 323 K and −4 V (vs Ag) for 2 h

mainly contain Al, O, and Nd. The presence of Al is attributed to the cathode substrate, while 21.91 wt.% Nd is derived from the reduction of Nd(III) in the solvated ionic liquid. In addition, the presence of O is mainly due to the high activity and small particle size of metallic Nd, which causes the oxidation of the electrodeposit upon exposure to air. However, within the resolution of the XRD detector, no Nd was detected, suggesting that the Nd deposit was non-crystalline [14−16]. In addition to SEM-EDS analysis, the electrodeposit was analyzed by XPS. In the fine scan of the Nd peak (Fig. 8(b)), 67.51 wt.% Nd was detected [35,36], revealing that metallic Nd was obtained by electrodeposition at −4 V (vs Ag) in the DMI−$LiNO_3$−$Nd(CF_3SO_3)_3$ solvated ionic liquid.

4 Conclusions

(1) The solvated ionic liquid comprising DMI and 0.5 mol/L $LiNO_3$ is suitable for the electrochemical preparation of Nd films from the $Nd(CF_3SO_3)_3$ precursor at room temperature.

(2) The density of the DMI−$LiNO_3$ solvated ionic liquid is 1.087−1.133 g/cm^3 at 298−358 K, which can be described by ρ=−7.64×10^{-4}T+1.36.

(3) The conductivities and viscosities of the DMI−$LiNO_3$ solvated ionic liquid are equal to 1.02−6.14 mS/cm at 301−350 K and 14.89−69.59 mPa·s at 298−348 K, respectively, which can be described by the following equations: σ=611530.43exp(−4032.58/T); ln η=−8.59+3825.7/T.

(4) The electrochemical reduction of Nd(III) is an irreversible diffusion-controlled process with a diffusion coefficient of 5.08×10^{-8} cm^2/s, which can be described as Nd(Ⅲ)+3e=Nd. EDS and XPS analyses of the electrodeposit at −4 V (vs Ag) confirm the presence of metallic Nd.

Acknowledgments

The authors are grateful for the financial supports from the National Natural Science Foundation of China (Nos. 52004062, 52074084, 51804070), the Natural Science Foundation of Liaoning Province of China (No. 2020-MS-084), and the Guangxi Innovation-Driven Development Program, China (No. GUIKE AA18118030).

References

[1] LAN Xi, GAO Jin-tao, DU Yu, GUO Zhan-cheng. Mineral evolution and separation of rare-earth phases from Bayan Obo rare-earth concentrate in a super-gravity field [J]. Journal of Alloys and Compounds, 2018, 731: 873−880.

[2] ALMESSIERE M A, KORKMAZ A D, SLIMANI Y, NAWAZ M, ALI S, BAYKAL A. Magneto-optical properties

of rare earth metals substituted Co−Zn spinel nanoferrites [J]. Ceramics International, 2019, 45(3): 3449−3458.

[3] GILANI Z A, WARSI M F, ANJUM M N, SHAKIR I, NASEEM S, RIAZ S, KHAN M A. Structural and electromagnetic behavior evaluation of Nd-doped lithium–cobalt nanocrystals for recording media applications [J]. Journal of Alloys and Compounds, 2015, 639: 268−273.

[4] SRIGURUNATHAN K, MEENAMBAL R, GULERIA A, KUMAR D, FERREIRA J M D F, KANNAN S. Unveiling the effects of rare-earth substitutions on the structure, mechanical, optical, and imaging features of ZrO_2 for biomedical applications [J]. ACS Biomaterials Science and Engineering, 2019, 5(4): 1725−1743.

[5] ZHANG Xiao-lian, YANG Chu-bin, LIU Hong-xia, PENG Guang-huai. Electrolytic preparation of Al−Sm alloy in SmF_3−LiF−Sm_2O_3 molten salt system [J]. Materials Science, 2019, 25(4): 466−470.

[6] ZHU Xiao-ping, SUN Shu-chen, LU Shuai-dan, HUANG Xiao-xiao, LI Kuan-he, TU Gan-feng, HUANG Xiao-wei, HUANG Shao-dong. Surface tension of light rare earth fluoride molten salts electrolyte system [J]. Thermochimica Acta, 2016, 636: 42−47.

[7] TSUDA T, NOHIRA T, ITO Y. Electrodeposition of lanthanum in lanthanum chloride saturated $AlCl_3$ 1-ethyl-3-methylinudazolium chloride molten salts [J]. Electrochimica Acta, 2001, 46(12): 1891−1897.

[8] LEGEAI S, DILIBERTO S, STEIN N, BOULANGER C, ESTAGER J, PAPAICONOMOU N, DRAYE M. Room-temperature ionic liquid for lanthanum electrodeposition [J]. Electrochemistry Communications, 2008, 10(11): 1661−1664.

[9] KIM P, XIE Hong-wei, GU Hui-min, ZHAI Yu-chun. Electrochemical study on electrodeposition of La^{3+} in $EMIMBF_4$ ionic liquid [J]. Rare Metal Materials and Engineering, 2012, 41(4): 599−602. (in Chinese)

[10] KONDO H, MATSUMIYA M, TSUNASHIMA K, KODAMA S. Attempts to the electrodeposition of Nd from ionic liquids at elevated temperatures [J]. Electrochimica Acta, 2012, 66: 313−319.

[11] OTA H, MATSUMIYA M, SASAYA N, NISHIHATA K, TSUNASHIMA K. Investigation of electrodeposition behavior for Nd(III) in $[P_{2225}]$[TFSA] ionic liquid by EQCM methods with elevated temperatures [J]. Electrochimica Acta, 2016, 222: 20−26.

[12] MATSUMIYA M, KIKUCHI Y, YAMADA T, KAWAKAMI S. Extraction of rare earth ions by tri-*n*-butylphosphate/phosphonium ionic liquids and the feasibility of recovery by direct electrodeposition [J]. Separation and Purification Technology, 2014, 130: 91−101.

[13] MATSUMIYA M, ISHII M, KAZAMA R, KAWAKAMI S. Electrochemical analyses of diffusion behaviors and nucleation mechanisms for neodymium complexes in [DEME][TFSA] ionic liquid [J]. Electrochimica Acta, 2014, 146: 371−377.

[14] GUO Cheng-yu, WANG Jian-chao, CHEN Bi-qing, WANG Jing-gui. Electrochemical studies on La−Co alloy film in acetamide−urea−NaBr melt system [J]. Transactions of Nonferrous Metals Society of China, 2005, 15(5): 1190−1193.

[15] GUO Cheng-yu, WANG Jian-chao, WANG Jing-gui, CHEN Bi-qing. Electrochemical preparation of La−Ni alloy film in acetamide−urea−NaBr melting system [J]. Journal of Rare Earths, 2005, 23(S1): 441−444.

[16] LIU Peng, DU Yu-ping, YANG Qi-qin, LI Gao-ren, TONG Ye-xiang. Electrochemical behavior of Fe(II) in acetamide−urea−NaBr−KBr melt and magnetic properties of inductively codeposited Nd−Fe film [J]. Electrochimica Acta, 2006, 52(2): 710−714.

[17] YANG Ying-ya, XU Cun-ying, HUA Yi-xin, WANG Meng-meng, SU Zhao-lei. Electrochemical preparation of Ni−La alloys from the EMIC−EG eutectic-based ionic liquid [J]. Ionics, 2017, 23(7): 1703−1710.

[18] ZHANG Bao-guo, SHI Zhong-ning, SHEN Ling-ling, LIU Xiao-zhen, XU Jun-li, WANG Zhao-wen. Low-temperature electrochemical codeposition of aluminum−neodymium alloy in a highly stable solvate ionic liquid [J]. Journal of Solid State Electrochemistry, 2019, 23(6): 1903−1909.

[19] ZHANG Bao-guo, YAO Yu, SHI Zhong-ning, XU Jun-li, LIU Xiao-zhen, WANG Zhao-wen. Direct room-temperature electrodeposition of La from $LaCl_3$ in an organic solvent supported by $LiNO_3$ [J]. Journal of the Electrochemical Society, 2019, 166(6): D218−D220.

[20] LIU Cheng-yuan, CHEN Wen-ting, WU Zi-mo, GAO Bing-liang, HU Xian-wei, SHI Zhong-ning, WANG Zhao-wen. Density, viscosity and electrical conductivity of $AlCl_3$−amide ionic liquid analogues [J]. Journal of Molecular Liquids, 2017, 247: 57−63.

[21] LIU Feng-guo, ZHONG Xiong-wei, XU Jun-li, KAMALI A, SHI Zhong-ning. Temperature dependence on density, viscosity, and electrical conductivity of ionic liquid 1-ethyl-3-methylimidazolium fluoride [J]. Applied Sciences, 2018, 8(3): 356.

[22] LI Min, GAO Bing-liang, CHEN Wen-ting, LIU Chen-yuan, WANG Zhao-wen, SHI Zhong-ning, HU Xian-wei. Electrodeposition behavior of aluminum from urea−acetamide−lithium halide low-temperature molten salts [J]. Electrochimica Acta, 2015, 185: 148−155.

[23] JOHANSSON P, FAST L E, MATIC A, APPETECCHI G B, PASSERINI S. The conductivity of pyrrolidinium and sulfonylimide-based ionic liquids: A combined experimental and computational study [J]. Journal of Power Sources, 2010, 195(7): 2074−2076.

[24] NISHIDA T, TASHIRO Y, YAMAMOTO M. Physical and electrochemical properties of 1-alkyl-3-methylimidazolium tetrafluoroborate for electrolyte [J]. Journal of Fluorine Chemistry, 2002, 120(2): 135−141.

[25] LI Min, GAO Bing-liang, LIU Chen-yuan, CHEN Wen-ting, WANG Zhao-wen, SHI Zhong-ning, HU Xian-wei. $AlCl_3$/amide ionic liquids for electrodeposition of aluminum [J]. Journal of Solid State Electrochemistry, 2016, 21(2): 469−476.

[26] BARGHAMADI M, BEST A S, HOLLENKAMP A F, MAHON P, MUSAMEH M, RÜTHER T. Optimising the concentration of $LiNO_3$ additive in C_4mpyr-TFSI electrolyte-based Li−S battery [J]. Electrochimica Acta, 2016, 222: 257−263.

[27] BARGHAMADI M, BEST A S, BHATT A I, HOLLENKAMP A F, MAHON P J, MUSAMEH M, RÜTHER T. Effect of $LiNO_3$ additive and pyrrolidinium ionic liquid on the solid electrolyte interphase in the lithiumesulfur battery [J]. Journal of Power Sources, 2015, 295: 212−220.

[28] SHAMSIPUR M, BEIGI A A M, TEYMOURI M, POURMORTAZAVI S M, IRANDOUST M. Physical and electrochemical properties of ionic liquids 1-ethyl-3- methyl-imidazolium tetrafluoroborate, 1-butyl-3-methyl- imidazolium trifluoromethanesulfonate and 1-butyl-1-methylpyrro-lidinium bis(trifluoromethylsulfonyl)imide [J]. Journal of Molecular Liquids, 2010, 157(1): 43−50.

[29] MALHAM I B, TURMINE M. Viscosities and refractive indices of binary mixtures of 1-butyl-3-methylimidazolium tetrafluoroborate and 1-butyl-2,3-dimethylimidazolium tetra-fluoroborate with water at 298 K [J]. Journal of Chemical Thermodynamics, 2008, 40(4): 718−723.

[30] XIE Yu-jiao, DONG Hai-feng, ZHANG Suo-jiang, LU Xiao-hua, JI Xiao-yan. Effect of water on the density, viscosity, and CO_2 solubility in choline chloride/urea [J]. Journal of Chemical and Engineering Data, 2014, 59(11): 3344−3352.

[31] CHEMAT F, ANJUM H, SHARIFF A M, KUMAR P, MURUGESAN T. Thermal and physical properties of (choline chloride + urea + *L*-arginine) deep eutectic solvents [J]. Journal of Molecular Liquids, 2016, 218: 301−308.

[32] LIU Ai-min, GUO Meng-xia, LÜ Zi-yang, ZHANG Bao-guo, LIU Feng-guo, TAO Wen-ju, YANG You-jian, HU Xian-wei, WANG Zhao-wen, LIU Yu-bao, SHI Zhong-ning. Electrochemical behavior of tantalum in ethylene carbonate and aluminum chloride solvate ionic liquid [J]. Transactions of Nonferrous Metals Society of China, 2020, 30(8): 2283−2292.

[33] BARD A J, FAULKNER R L. Electrochemical methods fundamentals and applications [M]. 2nd ed. New York: John Wiley & Sons, Inc., 2001.

[34] YAO K P, KWABI D G, QUINLAN R A, MANSOUR A N, GRIMAUD A, LEE Y L, LU Y C, YANG S H. Thermal stability of Li_2O_2 and Li_2O for Li-air batteries: In situ XRD and XPS studies [J]. Journal of the Electrochemical Society, 2013, 160(6): A824−A831.

[35] IWANOWSKI R J, HEINONEN M H, PRACKA I, KACHNIARZ J. XPS characterization of single crystalline $SrLaGa_3O_7$:Nd [J]. Applied Surface Science, 2013, 283: 168−174.

[36] KUMAR B V, VELCHURI R, PRASAD G, SREEDHAR B, RAVIKUMAR K, VITHAL M. Preparation, characterization, photoactivity and XPS studies of Ln_2ZrTiO_7 (Ln=Sm and Nd) [J]. Ceramics International, 2010, 36: 1347−1355.

DMI−$LiNO_3$溶剂化离子液体的物理化学性质及其在室温电沉积钕中的应用

刘爱民[1]，姚 宇[1]，郭梦霞[1]，刘玉宝[2]，石忠宁[3]，刘风国[1]，胡宪伟[1]，何文才[1]，王兆文[1]

1. 东北大学 多金属共生矿生态化冶金教育部重点实验室，沈阳 110819；
2. 包头稀土研究院 白云鄂博稀土资源研究与综合利用国家重点实验室，包头 014030；
3. 东北大学 轧制技术及连轧自动化国家重点实验室，沈阳 110819

摘 要：测定 1,3-二甲基-2-咪唑啉酮和硝酸锂(DMI−$LiNO_3$)溶剂化离子液体在不同温度下的密度、电导率和黏度，并研究 DMI−$LiNO_3$ 溶剂化离子液体中电沉积钕及其电化学机理。循环伏安结果表明，Nd(III)的电化学还原为不可逆的一步转移 3 个电子的过程，且受扩散控制，其扩散系数为 5.08×10^{-8} cm^2/s。能量分散 X 射线光谱和 X 射线光电子能谱分析表明，在 DMI−$LiNO_3$−$Nd(CF_3SO_3)_3$ 溶剂化离子液体及−4 V (vs Ag)条件下的电沉积产物包括金属钕。

关键词：电沉积；钕；离子液体；物理化学性质；循环伏安法

(Edited by Wei-ping CHEN)